Connections between Spring Arctic Ozone and the Summer Circulation and Sea Surface Temperatures over the Western North Pacific

TAO WANG, WENSHOU TIAN, JIANKAI ZHANG

Key Laboratory for Semi-Arid Climate Change of the Ministry of Education, College of Atmospheric Sciences, Lanzhou University, China

FEI XIE

College of Global Change and Earth System Science, Beijing Normal University, Beijing, China

RUHUA ZHANG, JINGLONG HUANG

Key Laboratory for Semi-Arid Climate Change of the Ministry of Education, College of Atmospheric Sciences, Lanzhou University, China

DINGZHU HU

Key Laboratory of Meteorological Disasters of China Ministry of Education (KLME)/Joint International Research Laboratory of Climate and Environment Change (ILCEC)/Collaborative Innovation Center on Forecast and Evaluation of Meteorological Disasters (CIC-FEMD), Nanjing University of Information Science &Technology, Nanjing 210044, China

*Correspondence to: wstian@lzu.edu.cn

Early Online Release: This preliminary version has been accepted for publication in *Journal of Climate*, may be fully cited, and has been assigned DOI 10.1175/JCLI-D-19-0292.1. The final typeset copyedited article will replace the EOR at the above DOI when it is published.

Abstract

Using various observations, reanalysis datasets, and a general circulation model (CESM-WACCM4), the relationship between the Arctic total column ozone (TCO) and the tropospheric circulation and sea surface temperatures (SSTs) over the western North Pacific (30°–45°N, 130°E–170°W) was investigated. We find that anomalies in the circulation and SSTs over the western North Pacific in June are closely related to anomalies in the Arctic TCO in March, i.e., when the Arctic TCO in March decreases, the anomalous tropospheric cyclone and negative SST anomalies (SSTAs) will occur over the western North Pacific in June. Further analysis indicates that the decreased Arctic TCO in March tends to result in a positive Victoria mode-like (VM) SSTAs over the North Pacific in April, which persist and develop an anomalous cyclone over the eastern North Pacific in May via atmosphere-ocean coupling. This anomalous cyclone over the eastern North Pacific subsequently induces an anomalous cyclone over the western North Pacific in June via westward-propagating Rossby waves in the lower troposphere. Furthermore, the negative SSTAs over the western North Pacific are enhanced by the anomalous northerly related to the anomalous cyclone in June. The effects of increased Arctic TCO in March on the tropospheric circulation and SSTs are almost opposite to those of decreased Arctic TCO. These results are also supported by our numerical simulations. Moreover, 10–20% of the anomalies in the tropospheric circulation and SSTs over the western North Pacific in June are contributed by the anomalies in the Arctic TCO in March.

Accepted for publication in *Journal of Climate*. DOI10.1175/JCLI-D-19-0292.1.

***Keywords**: Arctic stratospheric ozone, stratospheric polar vortex, stratosphere-troposphere coupling, Victoria Mode*

1. Introduction

Previous studies have reported that stratospheric circulation anomalies have an important effect on the tropospheric weather and climate (e.g., Baldwin and Dunkerton 2001; Graf and Walter 2005; Scaife et al. 2005; Cagnazzo and Manzini 2009; Ineson and Scaife 2009; Thompson et al. 2011; Reichler et al. 2012; Kidston et al. 2015; Sheng et al. 2015; Li et al. 2016; Zhang et al. 2016, 2018; Huang et al. 2017; Waugh et al. 2017). As a vital chemical component of the stratosphere, the loss and recovery of stratospheric ozone can affect, to a large degree, the stratospheric circulation through radiative processes (e.g., Ramaswamy et al. 1996; Labitzke and Naujokat 2000; Hu and Tung 2002; Tian et al. 2010; Hu et al. 2015). Thus, variations in the stratospheric ozone play an important role in the tropospheric climate change by influencing the stratospheric circulation (e.g., Hu and Tung 2003; Xie et al. 2016; Ivy et al. 2017; Garfinkel 2017).

The influence of Antarctic stratospheric ozone on the tropospheric climate change is a well-studied topic (e.g., Crook et al. 2007; Son et al. 2008; Waugh et al. 2009, 2015; Feldstein 2011; Hu et al. 2011; Kang et al. 2011; Gerber and Son 2014; Seviour et al. 2016; Xia et al. 2016) due to dramatic Antarctic stratospheric ozone loss (Farman et al. 1985; Ravishankara et al. 1994, 2009; Pawson and Naujokat 1999;

Accepted for publication in *Journal of Climate*. DOI10.1175/JCLI-D-19-0292.1.

Randel and Wu 1999, 2007; Solomon 1990, 1999). Antarctic ozone loss and the resulting ozone hole can induce a decrease in the Antarctic stratospheric temperature through radiative cooling (e.g., Randel and Wu 1999), which strengthens the Antarctic polar vortex. Furthermore, the strengthened westerlies associated with the Antarctic polar vortex extend downward from the stratosphere to surface and lead to the surface temperature changes over the Antarctic continent (Turner et al. 2005; Marshall et al. 2006). Many observations and simulations have demonstrated that the Antarctic ozone hole causes a poleward shift in the extratropical jet (Son et al. 2009, 2010), which is associated with a poleward shift in the subtropical dry and precipitation zones (Son et al. 2009; Polvani et al. 2011; Feldstein 2011; Kang et al. 2011), the extension of the Hadley cell (Min and Son 2013; Gerber and Son 2014; Waugh et al. 2015) and even changes in the ocean circulation (Russell et al. 2006; Bitz and Polvani 2012) in austral summer in the Southern Hemisphere (SH). In addition, the Antarctic stratospheric ozone also has effects on regional features of the SH climate, such as the Amundsen Sea Low (England et al. 2016) and Antarctic precipitation (Lenaerts et al. 2018).

Although the multidecadal loss of Arctic ozone is much smaller than that of Antarctic ozone (WMO, 2011), the interannual variability of Arctic TCO is large due to the variability of stratospheric polar vortex (e.g., Solomon et al. 2014, Ivy et al. 2017). The years 1997 and 2011 exhibited the most severe ozone depletion ever recorded over the Arctic (Lefèvre et al. 1998; Coy et al. 1997; Manney et al. 2011). Thus, the influence of Arctic stratospheric ozone on the tropospheric climate has

Accepted for publication in *Journal of Climate*. DOI10.1175/JCLI-D-19-0292.1.

received increasing attention. However, there does not seem to be overwhelming consensus in the literature on the size and robustness of the effects of spring Arctic ozone at present, which may be related to the amplitudes of ozone change and model used in different studies. Cheung et al. (2014) used the stratospheric ozone anomalies to predict the tropospheric climate related to ozone changes and found that the tropospheric forecast errors in the medium-extended range are dominated by the spread of ensemble members. Using a general atmospheric circulation model, Karpechko et al. (2014) found that the tropospheric impacts largely come from the SSTs and the ozone anomalies seem to play a minor role. Based on model studies, Smith and Polvani (2014) found that for ozone anomaly amplitudes within the observed range of the last three decades, their model experiments do not show statistically significant impacts at the surface, while extreme Arctic ozone has a significant effect on tropospheric circulation, surface temperature and precipitation. Subsequently, using a fully coupled stratosphere-resolving atmospheric model, Calvo et al. (2015) found that changes in the Arctic ozone induce large and robust anomalies in April-May tropospheric wind, temperature and precipitation over large parts of the Northern Hemisphere (NH). Ivy et al. (2017) presented observational evidence for a connection between the Arctic stratospheric ozone in March and the tropospheric climate and found that the stratospheric ozone is a useful predictor of spring tropospheric climate in some regions of the NH. Xie et al. (2016, 2017a, 2017b) reported that the Arctic stratospheric ozone variations in March lead to SSTAs similar

Accepted for publication in *Journal of Climate*. DOI10.1175/JCLI-D-19-0292.1.

to Victoria mode (VM) over the North Pacific in April and further influence El Niño Southern Oscillation (ENSO) and tropical rainfall, which lag ozone changes by approximately 20 months. More recently, studies found that spring Arctic stratospheric ozone has effects on local precipitation in China (Xie et al. 2018) and in the northwestern United States (Ma et al. 2019). As mentioned above, many studies reported the effects of spring Arctic ozone on springtime climate in NH, however, the effects of ozone on summertime climate in NH have not been clarified.

The Victoria mode (VM) is the second leading mode of SSTs over the North Pacific (Bond et al. 2003). The VM is closely related to marine ecosystem in North Pacific (e.g., Chenillat et al. 2012) and has important effects on climate, such as the South China Sea summer monsoon (Ding et al. 2018), precipitation (Ding et al. 2015a), tropical cyclones (Pu et al. 2019), and ENSO (e.g., Ding et al. 2015b, Xie et al. 2016), which further influences global climate (e.g., Kumar et al. 1999; Wang et al. 2000). Previous studies (e.g., Song et al. 2016) indicated that winter and spring VM anomalies can persist into summer through atmosphere-ocean coupling. Although many studies have found that changes in the Arctic stratospheric ozone influence the tropospheric climate in spring, it is unclear whether the effects of spring Arctic ozone on the tropospheric climate in the NH could persist into summer. If so, what are the associated mechanisms of the Arctic TCO variations in spring that impact summertime climate and to what extent do changes in the Arctic TCO affect the tropospheric summertime climate? Thus, in this paper, we analyze the impact of the

Accepted for publication in *Journal of Climate*. DOI10.1175/JCLI-D-19-0292.1.

Arctic TCO variations in March on the atmospheric circulation and SSTs over the North Pacific in early summer (June) and their associated mechanisms.

This paper is organized as follows. Section 2 describes methods and data. Section 3 analyzes the connections between Arctic TCO in March and the circulation and SSTs over the western North Pacific in June, as well as their underlying mechanisms. Section 4 gives the results of numerical simulations with high and low ozone conditions. Section 5 quantities the extent to which the variations of circulation and SSTs over the western North Pacific in June are explained by the March Arctic TCO changes. In Section 6, the conclusions and discussions are given.

2. Methods and data

a. Observations and reanalysis datasets

The TCO data are from the total ozone mapping spectrometer (TOMS)/solar backscatter ultraviolet (SBUV) dataset (Stolarski and Frith 2006) at a horizontal resolution of 5° x 10° (latitude x longitude). The TCO data from the MSR (multi-sensor reanalysis) dataset (van der et al. 2010, 2015), with a horizontal resolution of 0.5° x 0.5° (latitude x longitude), are also used in this paper. Figure 1 shows the time series of the Arctic (60°–90°N) TCO in March in the TOMS/SBUV dataset and MSR dataset, and these two datasets show good consistency in describing the interannual variability of Arctic TCO. Note that in this paper, before calculating correlation coefficients between the Arctic TCO in March and other variables, the

Accepted for publication in *Journal of Climate*. DOI10.1175/JCLI-D-19-0292.1.

TCO value is multiplied by –1 so that a positive correlation corresponds to positive anomalies in Arctic TCO with decreasing years.

The SST data are obtained from the UK Met Office Hadley Centre for Climate Prediction and Research SST (HadSST) dataset and Extended Reconstructed Sea Surface Temperature version4 (ERSSTv4). Geopotential height, temperature, and zonal and meridional wind are obtained from the European Centre for Medium-Range Weather Forecasts (ECMWF) Reanalysis-Interim (ERA-Interim) dataset and National Centers for Environmental Prediction 2 (NCEP2) reanalysis data from the US Department of Energy. Data used in this paper are monthly mean for the period 1979–2011.

b. Model simulations

The model used in this paper is the National Center for Atmospheric Research’s Community Earth System Model (CESM) version 1.2.2. CESM is a fully coupled global climate model that incorporates an interactive atmosphere (CAM/WACCM) component, ocean (POP2), land (CLM4), and sea ice (CICE). For the atmospheric component, we used the Whole Atmosphere Community Climate Model (WACCM), version 4 (Marsh et al. 2013). WACCM4 is a climate model that has detailed middle-atmosphere chemistry and a finite volume dynamical core, and it extends from the surface to approximately 140 km. For our study, we disabled the interactive chemistry in order to analyze the impact of stratospheric ozone changes in a specific

Accepted for publication in *Journal of Climate*. DOI10.1175/JCLI-D-19-0292.1.

month on the tropospheric circulations. WACCM4 has 66 vertical levels, with a vertical resolution of about 1 km in the tropical tropopause and lower stratosphere layers. Our simulations used a horizontal resolution of 1.9°×2.5° (latitude×longitude) for the atmosphere and approximately the same for the ocean.

The original ozone data are from the CMIP5 ensemble mean ozone output (1955–2005) and can be downloaded at https://svn-ccsm-inputdata.cgd.ucar.edu/trunk/inputdata/atm/waccm/ub/ghg_forcing_1955-2005_CMIP5_EnsMean.c140414.nc, which are zonal mean ozone field. We performed 4 transient experiments (R1–R4) with prescribed high and low ozone scenarios to verify the influence of the stratospheric ozone on the tropospheric circulation and SSTs. Note that we used stratospheric ozone forcing with interannual variability in this study to obtain modeling results more close to the real atmosphere. The difference among these 4 runs is March ozone concentration in the Arctic region (60°–90°N) and the ozone concentrations are prescribed as shown in Table 1. Experiments R1 (ozone decreased by 15%) and R2 (ozone increased by 15%) are performed to see the effects of ozone within the observed range, and this ozone change is also similar to that in Xie et al. (2018) and Ma et al. (2019). Experiments R3 (ozone decreased by 25%) and R4 (ozone increased by 25%) are performed to see the effects of ozone with larger amplitude change. More details of the numerical simulations are listed in Table 1.

Accepted for publication in *Journal of Climate*. DOI10.1175/JCLI-D-19-0292.1.

c. Methods

To analyze the propagation of Rossby waves, wave ray paths (e.g., Karoly et al. 1983; Zhang et al. 2015) are calculated by solving the linear barotropic vorticity equation. In the mean flow $\overline{\psi}(x, y)$, the perturbation flow function satisfies Equation (1):

$$\omega = \overline{u}_M k + \overline{v}_M l + \frac{(l\partial\overline{q} / \partial x - k\partial\overline{q} / \partial y)}{k^2 + l^2} \quad (1)$$

where ω is angular frequency; $(\overline{u}_M, \overline{v}_M) = ((\overline{u}, \overline{v}) / \cos\theta)$ represent the time mean zonal wind and meridional wind under Mercator projection, respectively; θ represents latitude; k and l represent the zonal and meridional wavenumbers, respectively; and $\overline{q}$ represents the absolute vorticity. We can obtain four equations describing the group velocity (u_g, v_g) and wavenumber (k, l) (Karoly et al. 1983), which can be integrated to obtain wave ray paths. The background flow field is obtained from the climatological (1979–2009) mean wind field in May-June.

Pacific Decadal Oscillation (PDO, Mantua et al. 1997; Zhang et al. 1997) and Victoria Mode (VM, Bond et al. 2003) are the first and second mode of SSTAs over the North Pacific, respectively. According to the methods of Ding et al. (2015b), we calculate the first two modes (i.e., PDO and VM) of SSTAs over the North Pacific (20.5°N–65.5°N, 124.5°E–100.5°W) in March by empirical orthogonal function (EOF) analysis.

To quantify the extent to which variations in the tropospheric circulation and SSTs over the western North Pacific in early summer (June) are explained by the

Accepted for publication in *Journal of Climate*. DOI10.1175/JCLI-D-19-0292.1.

Arctic TCO in March, we remove March SST signal from March Arctic TCO as shown in Equation (2):

$$\text{TCO (resi)} = \text{TCO} - \text{TCO (SST)} \qquad (2)$$

In Equation (2), TCO represents the original time series of the Arctic TCO in March. TCO (SST) is obtained by the regression of March PDO+VM index onto March Arctic TCO. Thus, the residual component of TCO, namely TCO (resi), is almost independent of March SSTs.

3. Connections between Arctic TCO variations in March and the tropospheric circulation and SST changes over the western North Pacific in early summer

Figure 2 shows the evolution of correlation coefficients between Arctic (60°–90°N) TCO in March and SSTs in March–August. Figure 2 indicates that the SSTAs in April (Fig. 2b) are similar to a positive VM, which is consistent with previous results (Xie et al. 2017a) that a decrease in the Arctic stratospheric ozone in March leads positive VM anomalies in April. Interestingly, the negative SSTAs over the western North Pacific (25°–40°N, 150°E–170°W) gradually weaken in May (Fig. 2c) but are suddenly enhanced and become statistically significant again in June (Fig. 2d). The amplitude of the negative SSTAs over the western North Pacific is strong, weak and strong in April, May and June (Figs. 2b–d), respectively. This phenomenon also exists in the MSR dataset and ERSSTv4 dataset (Figs. 2h–j), which supports the

Accepted for publication in *Journal of Climate*. DOI 10.1175/JCLI-D-19-0292.1.

robustness of this phenomenon. It is reasonable to presume that underlying processes related to the Arctic TCO changes in March enhance the amplitude of the negative SSTAs over the western North Pacific in June. Therefore, it is necessary to investigate the effects of the Arctic TCO in March on the tropospheric circulation and SSTs over the western North Pacific in June.

Figure 3 shows the correlation coefficients between the Arctic TCO in March and geopotential height and wind in June. Both the TOMS/SBUV dataset and MSR dataset indicate that there exist an anomalous tropospheric cyclonic flow and negative geopotential height anomalies associated with the decrease in March Arctic TCO over the western North Pacific in June (Fig. 3). The results of ERA-Interim dataset (Figs. 3a–b) and NCEP2 dataset (Figs. 3c–d) are similar, which indicates that these connections between the Arctic TCO in March and the circulation over the western North Pacific in June are reliable and not sensitive to dataset. Figure 4 shows the details of variations in the Arctic TCO in March and the upper tropospheric geopotential height, lower tropospheric geopotential height and SSTs over the western North Pacific from April to June. There are close connections between the Arctic TCO in March and the upper tropospheric geopotential height ($r=0.61$, $p<0.01$), lower tropospheric geopotential height ($r=0.53$, $p<0.01$) and SSTs ($r=0.47$, $p<0.01$) over the western North Pacific in April (Figs. 4a–c), which are consistent with the results in Xie et al. (2017a) that a decrease in March Arctic ozone leads geopotential height anomalies similar to negative NPO (North Pacific Oscillation) and SSTAs similar to

Accepted for publication in *Journal of Climate*. DOI10.1175/JCLI-D-19-0292.1.

positive VM over the North Pacific in April. Gradually, these correlation coefficients weaken in May (Figs. 4d–f). However, the connections between the Arctic TCO in March and the upper tropospheric geopotential height ($r=0.47$, $p<0.01$), lower tropospheric geopotential height ($r=0.46$, $p<0.01$) and SSTs ($r=0.55$, $p<0.01$) are enhanced and become statistically significant again in June (Figs. 4g–i).

The above results suggest close connections between the Arctic TCO in March and the tropospheric circulation and SSTs over the western North Pacific in June, and variations in the TCO lead variations in the circulation and SSTs by three months. These lead-lag connections suggest that changes in March Arctic TCO may affect the tropospheric circulation and SSTs over the western North Pacific in June. Therefore, a question arises as to what mechanism is responsible for these lead-lag connections. Considering that the results obtained from various datasets are similar, we only show the results of the TOMS/SBUV, ERA-Interim and HadSST datasets in the following text.

Figure 5 displays temperature and circulation anomalies associated with the Arctic TCO in March. A decrease in the Arctic TCO in March corresponds to a colder and stronger stratospheric polar vortex (SPV, Figs. 5a–c), indicating that the decrease in the Arctic TCO strengthens the SPV through radiative processes (e.g., Ramaswamy et al. 1996; Hu et al. 2011). Furthermore, the positive zonal wind anomalies extend downward into the lower troposphere (Fig. 5c) through wave-mean flow interactions (e.g., Haynes et al. 1991; Song et al. 2004; Chen et al. 2007; Garfinkel and Hartmann

Accepted for publication in *Journal of Climate*. DOI10.1175/JCLI-D-19-0292.1.

2011; Garfinkel et al. 2013). Note that correlation coefficients between March Arctic TCO and April and May Arctic TCO are 0.82 ($p<0.01$), 0.72 ($p<0.01$), respectively, suggesting the auto-correlation of Arctic ozone. However, the stratospheric circulation anomalies associated with April-May Arctic TCO are relatively weak and do not extend downward into the troposphere (not shown), indicating that the circulation and SST anomalies over the western North Pacific in June (Figs. 2–3) should be linked to the March ozone rather than the April/May ozone. Xie et al. (2017a) indicated that the positive zonal wind anomalies in the region 60°–90°N, 180°–120°W in March, caused by the decreased stratospheric ozone anomalies in March, contribute to negative North Pacific Oscillation (NPO) anomalies in April. It is evident that there are statistically significant circulation anomalies at high latitudes in March (Fig. 5d) and negative NPO anomalies in April (Fig. 5e), which force positive VM anomalies (Fig. 2b). Here, we investigate how April SSTAs over North Pacific related to the Arctic TCO affect the circulation and SSTs over the western North Pacific in June.

Figure 6 shows the evolution of correlation coefficients between Arctic TCO in March and the lower tropospheric geopotential height, wind and SSTs from April to June. The geopotential height anomalies similar to –NPO (Fig. 6d) and SST anomalies similar to +VM (Fig. 6a) are obvious and statistically significant in April. In addition, the April VM anomalies persist and develop into the next month (Fig. 6b) through atmosphere-ocean coupling (Xie and Philander 1994; Vimont et al. 2003; Song et al. 2016). Vimont et al. (2003) indicated that surface heating induced by the

Accepted for publication in *Journal of Climate*. DOI10.1175/JCLI-D-19-0292.1.

subtropical positive SSTAs over the eastern North Pacific leads to northward meridional flow over the positive SSTAs regions (15°–30°N, 160°–120°W; Fig. 6b) and, in turn, the northward meridional flow enhances the local positive SSTAs. The northward meridional flow could further result in a surface cyclonic flow centered over the northern and western regions (15°–40°N, 160°–120°W; Figs. 6b, e) of the subtropical positive SSTAs (Vimont et al. 2003). The features in Fig. 6b are also consistent with the results of Song et al. (2016, their Fig. 5b) describing the development of VM mode associated with an anomalous cyclone over the eastern North Pacific. In June, an anomalous cyclonic flow and enhanced negative SSTAs (Fig. 6c) occur over the western North Pacific compared to those in May.

Li et al. (2015, their Fig. 11) indicated that Rossby waves in mid-lower latitudes propagate westward in summertime lower troposphere. Therefore, it is reasonable that the anomalous cyclonic flow over the eastern North Pacific (15°–40°N, 160°–120°W) in May (Figs. 6b, e), associated with the decrease in the Arctic TCO in March, could affect the circulation over the western North Pacific at a certain lag time through westward-propagating Rossby waves. Figure 7 indicates that the lower tropospheric Rossby waves originated from the eastern North Pacific will propagate to the western North Pacific approximately one month later along the anticyclone path. These results confirm that the cyclonic circulation anomalies over the eastern North Pacific in May (Figs. 6b, e) have an effect on circulation over the western North Pacific in the subsequent June (Figs. 6c, f). To further explore this lead-lag effect, we calculate

Accepted for publication in *Journal of Climate*. DOI10.1175/JCLI-D-19-0292.1.

correlation coefficients between the geopotential height averaged over the eastern Pacific (30°–35°N, 145°–135°W) in May and geopotential height fields over the North Pacific in June as shown in Fig. 8. Figure 8 indicates that if there are negative geopotential height anomalies over the eastern North Pacific (15°–40°N, 160°–130°W) in May (Fig. 8a), there will be negative geopotential height anomalies over the western North Pacific in the subsequent June (Fig. 8b). Therefore, Fig. 8 further indicates that the tropospheric circulation changes over the western North Pacific in June are strongly linked to the circulation anomalies over the eastern North Pacific in May. Figures 7 and 8 indicate that the anomalous cyclone over the eastern North Pacific in May (Figs. 6b, e) induces the anomalous cyclone over the western North Pacific in June (Figs. 6c, f). Furthermore, the anomalous northerly over the western North Pacific (30°–40°N, 140°–180°E, Figs. 3b, d or Fig. 6c), associated with the anomalous cyclone, enhances the local negative SSTAs (Figs. 2d, j or Fig. 6c). Note that correlation coefficients between the Arctic TCO in March and net surface sensible and latent heat flux over the western North Pacific (30°–45°N, 130°E–170°W) in June are very small and not significant (not shown), suggesting that the effects of SSTAs in June over the western North Pacific on local atmosphere are weak.

Based on the above analysis, we propose a mechanism by which the Arctic TCO in March influences the circulation and SSTs over the western North Pacific in June. The mechanism includes the following processes: (1) A decrease in the Arctic TCO in

Accepted for publication in *Journal of Climate*. DOI10.1175/JCLI-D-19-0292.1.

March enhances the SPV (Fig. 5) and further induces negative NPO anomalies (Fig. 6d) and positive Victoria mode (VM) anomalies (Fig. 6a) in April, which has been clarified by previous studies (Xie et al. 2017a). (2) The April SSTAs associated with the decrease in Arctic TCO in March persist and develop an anomalous cyclone over the eastern North Pacific (15°–40°N, 160°–120°W) in May (Figs. 6b, e) through atmosphere-ocean coupling (e.g., Vimont et al. 2003; Song et al. 2016). (3) This anomalous cyclone (Figs. 6b, e) further leads to an anomalous cyclone over the western North Pacific in June (Figs. 6c, f) by westward-propagating Rossby waves in the lower troposphere, which would take approximately one month (Figs. 7–8). Furthermore, the anomalous northerly over the western North Pacific (30°–40°N, 140°–180°E, Figs. 3b, d or Fig. 6c) associated with the anomalous cyclone enhances the local negative SSTAs (Figs. 2d, j or Fig. 6c). The effects of an increase in Arctic TCO in March are almost opposite to those of a decrease in March Arctic TCO.

4. Simulated variations in circulation and SSTs forced by spring Arctic ozone anomalies.

In this section, we use numerical simulations to verify the results obtained from the reanalysis data. The model and experiments are introduced in Section 2. Figure 9 shows the ozone forcing prescribed in experiments R1–R4. Figure 10 shows the geopotential height and SST differences between experiments R1 (ozone decreased by 15%) and R2 (ozone increased by 15%). It is apparent that a 15% stratospheric ozone

Accepted for publication in *Journal of Climate*. DOI10.1175/JCLI-D-19-0292.1.

decrease induces negative SST anomalies over the middle North Pacific (20°–30°N, 120°E–150°W) and positive SST anomalies over the northern, eastern and southern North Pacific in April (Fig. 10a), which is similar to the VM. The pattern of geopotential height in April is similar to NPO (Fig. 10d), with a negative center over southern regions (15°–35°N, 160°E–150°W) of North Pacific and a positive center over the northern regions (40°–60°N, 160°E–140°W). Although the centers of the NPO and VM in Figs. 10a, d are located further south than those in the reanalysis dataset (Figs. 6a, d), their patterns are overall similar. Figs. 10a, d support the result that the stratospheric ozone decrease in March could induce NPO and VM anomalies over the North Pacific in April.

Comparing experiments R1 and R2, the model cannot capture the ozone-related negative geopotential height anomalies and the enhanced negative SSTs over the western North Pacific in June as exhibited in the reanalysis data (Figs. 6c, f). This may be because that the differences in VM anomaly between experiments R1 and R2 are weak (Fig. 10a). Especially, positive SSTAs over the eastern North Pacific regions (10°–30°N, 160°–120°W; Fig. 10a) are weak so that the development of cyclonic circulation anomaly over the eastern North Pacific (10°–30°N, 160°–120°W) is not standout (Figs. 10b, e), which is a key process that induces the cyclonic circulation anomaly and enhanced negative SST anomalies over the western North Pacific in June as shown in Figs. 6b, e. Therefore, the anomalous cyclonic flow and enhanced negative SST anomalies over the western North Pacific in June are also not

Accepted for publication in *Journal of Climate*. DOI10.1175/JCLI-D-19-0292.1.

reproduced by the model experiments (Figs. 10c, f). Thus, we performed another two numerical experiments (R3 and R4) to see if a larger ozone decrease can induce the circulation and SST anomalies in June.

Figure 11 shows the geopotential height and SST differences between experiments R3 (ozone decreased by 25%) and R4 (ozone increased by 25%). Similar to the results of experiments R1 and R2, there are still ozone-induced NPO and VM anomalies over the North Pacific in April (Figs. 11a, d), and the SST differences (Fig. 11a) are larger than that in experiments R1–R2 (Fig. 10a). Furthermore, these experiments can capture the development of the anomalous cyclone over the eastern North Pacific (20°–40°N, 180°–140°W) in May (Figs. 11b, e) induced by the ozone decrease and the subsequent ozone-induced anomalous cyclone over the western North Pacific (30°–50°N, 120°–140°E) in June (Figs. 11c, f), supporting the results in reanalysis data that the VM anomaly associated with March Arctic ozone induces an anomalous cyclone over the western North Pacific in June (Figs. 6c, f). Note that the negative SST anomalies over the western North Pacific (30°–50°N, 130°E–180°) in June (Fig. 11c) are not enhanced compared to that in May (Fig. 11b), which may be because that the position of the anomalous cyclone is further west (30°–50°N, 120°–140°E, Fig. 11f) than those in the reanalysis data (Fig. 6f).

Figure 10 suggests that the simulation with a 15% ozone decrease reproduces too weak VM anomaly in April (Fig. 10a) to induce the anomalous cyclone over the western North Pacific in June, which may be related to the limitation in model ability

Accepted for publication in *Journal of Climate*. DOI10.1175/JCLI-D-19-0292.1.

to simulate the air-sea feedback processes over North Pacific. However, when the amplitude of ozone change is increased to 25%, the model could reproduce a large VM anomaly in April (Fig. 11a) and the subsequent anomalous cyclones in May and June (Figs. 11e, f), which are similar to that in the reanalysis data (Fig. 6). Both Fig. 10 and Fig. 11 indicate that stratospheric ozone changes in March contribute to VM anomaly over North Pacific in April and Fig. 11 further supports the rationality of the mechanism proposed in this study.

5. Contribution of the Arctic TCO variations in March to changes in the circulation and SSTs over the western North Pacific in early summer

In this section, we quantify the extent to which the variation in the tropospheric circulation and SSTs over the western North Pacific in early summer (June) could be explained by the Arctic TCO in March. Note that there likely exists a bi-directional connection in March between the Arctic TCO and the SSTs over the North Pacific, i.e., the SSTs in March (Fig. 2a) may affect stratospheric ozone. Therefore, we check the relationship in March between SST and Arctic TCO. The spatial patterns of PDO and VM are shown in Fig. 12a and Fig. 12b, respectively. It is found that correlation coefficients between the Arctic TCO in March and PDO and VM are –0.36 ($p<0.05$) and –0.39 ($p<0.05$), respectively (Figs. 12c–d). The correlation coefficient between the Arctic TCO and PDO+VM is –0.53 ($p<0.01$). The statistically significant

Accepted for publication in *Journal of Climate*. DOI10.1175/JCLI-D-19-0292.1.

correlation coefficient in March between Arctic TCO and SSTs is likely linked to the effects of North Pacific SSTs on the stratospheric polar vortex (Jadin et al. 2010; Hurwitz et al. 2012; Garfinkel et al. 2015; Woo et al. 2015; Kren et al. 2016; Hu et al. 2018; Hu and Guan 2018) and thereby the Arctic TCO (e.g., Schoeberl and Hartmann 1991). Therefore, to accurately estimate the extent to which the variations in the tropospheric circulation and SSTs over the western North Pacific in June are explained by the Arctic TCO changes in March, we first remove March SST signal from March Arctic TCO using a linear regression model as shown in Equation (2).

Figure 13 shows the correlation coefficients between the TCO (resi) in March and the tropospheric circulation and SSTs over the western North Pacific in June. Although the correlation coefficients in Fig. 13 are smaller than those in Figs. 2–3, statistically significant negative correlation coefficients still exist over the western North Pacific (Figs. 13a–c), which further indicates that a decrease in the Arctic TCO in March leads to the tropospheric cyclonic circulation anomalies and negative SSTAs over the western North Pacific in June and vice versa. Moreover, 10–20% of the variations in the tropospheric circulation and SSTs over the western North Pacific in June are contributed by the Arctic TCO variations in March (Figs. 13d–f).

6. Conclusions and discussions

In this study, various observations, reanalysis datasets, and a general circulation model (CESM-WACCM4) were used to probe the potential connections between

Accepted for publication in *Journal of Climate*. DOI10.1175/JCLI-D-19-0292.1.

TCO variations and the tropospheric circulation and SST changes. We found that the tropospheric cyclonic circulation anomalies and negative SSTAs over the western North Pacific (30°–45°N, 130°E–170°W) in June are closely linked to the decrease in Arctic TCO in March and vice versa. In addition, variations in the Arctic TCO in March lead the changes in the tropospheric circulation and SSTs over the western North Pacific by three months.

We further analyzed the underlying mechanism responsible for the lead-lag correlations between the Arctic TCO in March and the tropospheric circulation and SSTs over the western North Pacific in June. The main mechanisms are as follows: (1) A decrease in the Arctic TCO in March strengthens the stratospheric polar vortex (Figs. 5a–c) and further induces negative NPO anomalies (Fig. 6d) and positive Victoria mode (VM) anomalies (Fig. 6a) in April, which are consistent with previous study (Xie et al. 2017a). Subsequently, the April VM anomaly associated with the decrease in the Arctic TCO in March persists and develops an anomalous cyclone over the eastern North Pacific in May (Figs. 6b, e) through atmosphere-ocean coupling. (2) This anomalous cyclone over the eastern North Pacific in May (Figs. 6b, e) further causes an anomalous cyclonic flow over the western North Pacific in June (Figs. 6c, f) via westward-propagating Rossby waves in the lower troposphere, which would take approximately one month (Figs. 7–8). Furthermore, the anomalous northerly over western North Pacific (30°–40°N, 140°–180°E; Figs. 3b, d or Fig. 6c) associated with the anomalous cyclone enhances the local negative SSTAs (Figs. 2d, j

Accepted for publication in *Journal of Climate*. DOI10.1175/JCLI-D-19-0292.1.

or Fig. 6c). The effects of an increase in the Arctic TCO in March on the tropospheric circulation and SSTs over the western North Pacific are almost opposite to those of a decrease in March Arctic TCO.

The simulated results also indicate that the stratospheric ozone decrease contributes to NPO and VM anomalies over the North Pacific in April (Figs. 10a, d and Figs. 11a, d), which are helpful additions to previous results (Xie et al. 2016, 2017a). Moreover, the ozone-induced anomalous cyclones over the eastern North Pacific (20°–40°N, 180°–140°W) in May (Fig. 11e) and over the western North Pacific (30°–50°N, 120°–140°E) in June (Fig. 11f) further support the results in the reanalysis data that the positive VM anomaly associated with the stratospheric ozone decrease develops an anomalous cyclone over the eastern North Pacific in May (Figs. 6b, e) via atmosphere-ocean coupling, which further induces an anomalous cyclone over the western North Pacific in June (Figs. 6c, f) by westward-propagating Rossby waves (Fig. 7).

Our analysis indicates that 10–20% of the variations in the tropospheric circulation and SSTs over the western North Pacific in June are contributed by the Arctic TCO variations in March (Fig. 13), implying that the TCO variation in March could be a useful seasonal-timescale predictor of the tropospheric circulation and SST changes over the western North Pacific in early summer. The above results also imply that the SSTs over the western North Pacific in early summer may become warmer in the future due to stratospheric ozone recovery.

Accepted for publication in *Journal of Climate*. DOI10.1175/JCLI-D-19-0292.1.

Due to the large internal variability of Arctic climate, it is necessary to use a large enough ozone anomaly to distinguish robust atmospheric circulation change associated with stratospheric ozone changes from that driven by natural variability. In addition, the relationships between March Arctic TCO and the tropospheric circulation and SSTs in June are really strong in various observations and reanalysis datasets (Figs. 2–4). However, whether climate model runs underestimate the response remains unclear, which needs further study.

Acknowledgements

This work is supported by the Strategic Priority Research Program of Chinese Academy of Sciences (XDA17010106) and the National Natural Science Foundation of China (41630421, 41705022, and 41575038). We thank Institute Pierre Simon Laplace (IPSL) for access to the ERA-Interim data. We thank the scientific teams at NCEP and NCAR for providing the reanalysis data.

References

Baldwin, M. P., and T. J. Dunkerton, 2001: Stratospheric harbingers of anomalous weather regimes. *Science*, **294**, 581–584, https://doi.org/10.1126/science.1063315.

Bitz, C. M., and L. M. Polvani, 2012: Antarctic climate response to stratospheric ozone depletion in a fine resolution ocean climate model. *Geophys. R* *es. Lett.*, **39**, L20705, https://doi.org/10.1029/2012GL053393.

Bond, N. A., J. E. Overland, M. Spillane, and P. Stabeno, 2003: Recent shifts in the state of the North Pacific. *Geophys. Res. Lett.*, **30**, 2183, https://doi.org/10.1029/2003GL018597.

Cagnazzo, C., and E. Manzini, 2009: Impact of the stratosphere on the winter tropospheric teleconnections between ENSO and the North Atlantic and European region. *J. Climate*, **22**, 1223–1238. https://doi.org/10.1175/2008JCLI2549.1

Calvo, N., L. M. Polvani, and S. Solomon, 2015: On the surface impact of Arctic stratospheric ozone extremes. *Environ. Res. Lett.*, **10**, 094003, https://doi.org/10.1088/1748-9326/10/9/094003.

Chen, G., and I. M. Held, 2007: Phase speed spectra and the recent poleward shift of Southern Hemisphere surface westerlies. *Geophys. Res. Lett.*, **34**, L21805, https://doi.org/10.1029/2007GL031200.

Chenillat, F., P. Rivière, X. Capet, E. Di Lorenzo, and B. Blanke, 2012: North Pacific Gyre Oscillation modulates seasonal timing and ecosystem functioning in the California Current upwelling system. *Geophys. Res. Lett.*, **39**(1), https://doi.org/10.5194/acp-14-13705-2014.

Cheung, J. C. H., J. D. Haigh, and D. R. Jackson, 2014: Impact of EOS MLS ozone data on medium- extended range ensemble weather forecasts. *J. Geophys. Res. Atmos.*, **119**, 9253–9266, https://doi.org/10.1002/2014JD021

Accepted for publication in *Journal of Climate*. DOI10.1175/JCLI-D-19-0292.1.

823

Coy, L., E. Nash, and P. Newman, 1997: Meteorology of the polar vortex: Spring 1997. *Geophys. Res. Lett.*, **24**, 2693–2696, https://doi.org/10.1029/97GL52832.

Crook, J. A., N. P. Gillett, S. P. E. Keeley, 2008: Sensitivity of Southern Hemisphere climate to zonal asymmetry in ozone. *Geophys. Res. Lett.* , **35** (7). doi:10.1029/2007GL032698.

Ding R., and Coauthors, 2015a: Influence of the North Pacific Victoria mode on the Pacific ITCZ summer precipitation. *J. Geophys. Res. Atmos.*, **120** (3), 964-979, https://doi.org/Doi 10.1029/96jd03250.

Ding, R., J. Li, and Y.-H. Tseng, 2015b: The Victoria mode in the North Pacific linking extratropical sea level pressure variations to ENSO. *J. Geophys. Res. Atmos.*, **120**, 27–45, https://doi.org/10.1002/2014JD022221.

Ding, R., J. Li, Y.-H. Tseng, L. Li, C. Sun, and F. Xie, 2018: Influences of the North Pacific Victoria Mode on the South China Sea Summer Monsoon. *Atmosphere*, **9**(6): 229, https://doi.org/10.3390/Atmos9060229.

England, M., L. Polvani, K. Smith, L. Landrum, and M. Holland, 2016: Robust response of the Amundsen Sea Low to stratospheric ozone depletion, *Geophys. Res. Lett.*, **43**, 8207–8213, doi: 10.1002/2016GL070055

Farman, J. C., B. G. Gardiner, and J. D. Shanklin, 1985: Large Losses of Total Ozone in Antarctica Reveal Seasonal Clox/Nox Interaction. *Nature*, **3**

Accepted for publication in *Journal of Climate*. DOI10.1175/JCLI-D-19-0292.1.

15, 207–210, https://doi.org/10.1038/315207a0.

Feldstein, S. B., 2011: Subtropical Rainfall and the Antarctic Ozone Hole. *Science*, 2011, **332**, 925–926, https://doi.org/10.1126/science.1206834.

Garfinkel, C. I., and D. L. Hartmann, 2011: The influence of the quasi-biennial oscillation on the troposphere in winter in a hierarchy of models. Part II: Perpetual winter WACCM runs. *J. Atmos. Sci.*, **68**, 2026–41, https://doi.org/10.1175/2011JAS3702.1.

——, D. W. Waugh, and E. P. Gerber, 2013: The effect of tropospheric jet latitude on coupling between the stratospheric polar vortex and the troposphere. *J. Climate*, **26**, 2077–95, https://doi.org/10.1175/JCLI-D-12-00301.1.

——, M. M. Hurwitz, and L. D. Oman, 2015: Effect of recent sea surface temperature trends on the Arctic stratospheric vortex. *J. Geophys. Res. Atmos.*, **120**, 5404–5416, https://doi.org/10.1002/2015JD023284.

——, 2017: Might stratospheric variability lead to improved predictability of ENSO events? *Environ. Res. Lett.*, **12**, 031001, https://doi.org/10.1088/1748-9326/aa60a4.

Gerber, E. P., and S. W. Son, 2014: Quantifying the summertime response of the austral jet stream and Hadley cell to stratospheric ozone and greenhouse gases. *J. Climate*, **27**, 5538 - 5559, https://doi.org/10.1175/JCLI-D-13-00539.1.

Accepted for publication in *Journal of Climate*. DOI10.1175/JCLI-D-19-0292.1.

Graf, H. F., and K. Walter, 2005: Polar vortex controls coupling of North Atlantic Ocean and atmosphere. *Geophys. Res. Lett.*, **32**, L01704, https://doi.org/10.1029/2004GL020664.

Haynes, P. H., C. J. Marks, M. E. McIntyre, T. G. Shepherd, and K. P. Shine, 1991: On the “downward control” of extratropical diabatic circulations by eddy-induced mean zonal forces. *J. Atmos. Sci.*, **48**, 651–678, https://doi.org/10.1175/1520-0469(1991)048<0651:OTCOED>2.0.CO;2.

Huang, J., W. Tian, J. Zhang, Q. Huang, H. Tian, and J. Luo, 2017: The connection between extreme stratospheric polar vortex events and tropospheric blockings. *Quart. J. Roy. Meteor. Soc.*, **143**, 1148–1164, https://doi.org/10.1002/qj.3001.

Hu, D., W. Tian, F. Xie, C. Wang, and J. Zhang, 2015: Impacts of stratospheric ozone depletion and recovery on wave propagation in the boreal winter stratosphere. *J. Geophys. Res. Atmos.*, **120**, 8299–8317, https://doi.org/10.1002/2014JD022855.

——, and Z. Guan, 2018: Decadal Relationship between the Stratospheric Arctic Vortex and Pacific Decadal Oscillation. *J. Climate*, **31**, 3371–86, https://doi.org/10.1175/JCLI-D-17-0266.1.

——, Z. Guan, W. Tian, and R. Ren, 2018: Recent strengthening of the stratospheric Arctic vortex response to warming in the central North Pacific. *Nat. Commun.*, **9**, 1697, https://doi.org/10.1038/s41467-018-04138-3.

Accepted for publication in *Journal of Climate*. DOI 10.1175/JCLI-D-19-0292.1.

Hurwitz, M. M., P. A. Newman, and C. I. Garfinkel, 2012: On the influence of North Pacific sea surface temperature on the Arctic winter climate. *J. Geophys. Res.*, **117**, D19110, https://doi.org/10.1029/2012JD017819.

Hu, Y, and K. K. Tung, 2002: Interannual and decadal variations of planetary wave activity, stratospheric cooling, and Northern Hemisphere annular mode. *J. Climate*, **15**, 1659-1673, https://doi.org/10.1175/1520-0442(2002)015<1659:IADVOP>2.0.CO;2.

——, and ——, 2003: Possible ozone-induced long-term changes in planetary wave activity in late winter. *J. Climate*, **16**, 3027-3038, https://doi.org/10.1175/1520-0442(2003)016<3027:POLCIP>2.0.CO;2.

——, Y. Xia, and Q. Fu, 2011: Tropospheric temperature response to stratospheric ozone recovery in the 21st century. *Atmos. Chem. Phys.*, **11**, 7687–7699, https://doi.org/10.5194/acp-11-7687-2011.

Ineson, S., and A. A. Scaife, 2009: The role of the stratosphere in the European climate response to El Niño. *Nat. Geosci.*, **2**, 32–36. https://doi.org/10.1038/NGEO381.

Ivy, D. J., S. Solomon, N. Calvo, and D. W. Thompson, 2017: Observed connections of Arctic stratospheric ozone extremes to Northern Hemisphere surface climate. *Environ. Res. Lett.*, 2017, **12**, 024004, https://doi.org/10.1088/1748-9326/aa57a4.

Jadin, E. A., K. Wei, Y. A. Zyulyaeva, W. Chen, and L. Wang, 2010: Stratos

Accepted for publication in *Journal of Climate*. DOI 10.1175/JCLI-D-19-0292.1.

pheric wave activity and the Pacific decadal oscillation. *J. Atmos. Sol. Terr. Phys.*, **72**, 1163–1170, https://doi.org/10.1016/j.jastp.2010.07.009.

Kang, S. M., L. M. Polvani, J. C. Fyfe, and M. Sigmond, 2011: Impact of polar ozone depletion on subtropical precipitation. *Science*, **332**, 951–954, https://doi.org/10.1126/science.1202131.

Karoly, D. J., 1983: Rossby-wave propagation in a barotropic atmosphere. *Dyn. Atmos. Oceans*, **7**, 111–125., https://doi.org/10.1016/0377-0265(83)90013-1.

Karpechko, A. Y., J. Perlwitz, E. A. Manzini, 2014: A model study of tropospheric impacts of the Arctic ozone depletion 2011. *J. Geophys. Res. Atmos.*, **119**, 7999–8014, https://doi.org/10.1002/2013JD021350.

Kidston, J., A. A. Scaife, S. C. Hardiman, D. M. Mitchell, N. Butchart, M. P. Baldwin, and L. J. Gray, 2015: Stratospheric influence on tropospheric jet streams, storm tracks and surface weather. *Nat. Geosci.*, **8**, 433–440, https://doi.org/10.1038/ngeo2424.

Kren, A. C., D. R. Marsh, A. K. Smith, and P. Pilewskie, 2016: Wintertime Northern Hemisphere response in the stratosphere to the Pacific decadal oscillation using the Whole Atmosphere Community Climate Model. *J. Climate*, **29**, 1031–1049, https://doi.org/10.1175/JCLI-D-15-0176.1.

Kumar, K. K., B. Rajagopalan, and M. A. Cane., 1999: On the weakening relationship between the Indian monsoon and ENSO. *Science*, **284**(5423): 21

Accepted for publication in *Journal of Climate*. DOI10.1175/JCLI-D-19-0292.1.

56-2159, DOI 10.1126/science.284.5423.2156.

Labitzke, K., and B. Naujokat, 2000: The lower Arctic stratosphere in winter since 1952. *Sparc Newslett.*, **15**, 11–14.

Lefèvre, F., F. Figarol, K. S. Carslaw, and T. Peter, 1998: The 1997 Arctic ozone depletion quantified from three-dimensional model simulations. *Geophys. Res. Lett.*, **25**, 2425–2428, https://doi.org/10.1029/98GL51812.

Lenaerts, J. T. M., J. Fyke, and B. Medley, 2018: The signature of ozone depletion in recent Antarctic precipitation change: A study with the Community Earth System Model. *Geophys. Res. Lett.*, **45**, 12,931–12,939. https://doi.org/10.1029/2018GL078608.

Li, F., Y. V. Vikhliaev, P. A. Newman, S. Pawson, J. Perlwitz, D. W. Waugh, and A. R. Douglass, 2016: Impacts of Interactive Stratospheric Chemistry on Antarctic and Southern Ocean Climate Change in the Goddard Earth Observing System, Version 5 (GEOS-5). *J. Climate*, **29**, 3199–3218, https://doi.org/10.1175/Jcli-D-15-0572.1.

Li, Y., and J. Li, F. Jin, and S. Zhao, 2015: Interhemispheric propagation of stationary Rossby waves in the horizontally nonuniform background flow. *J. Atmos. Sci.*, **72**, 3233–3256, https://doi.org/10.1175/JAS-D-14-0239.1.

Manney, G., and Coauthors, 2011: Unprecedented Arctic ozone loss in 2011. *Nature*, **478**, 469－475, http://dx.doi.org/10.1594/PANGAEA.547983.

Mantua, N. J., S. R. Hare, Y. Zhang, J. M. Wallace, and R. C. Francis, 1997:

Accepted for publication in *Journal of Climate*. DOI10.1175/JCLI-D-19-0292.1.

A Pacific interdecadal climate oscillation with impacts on salmon production. *Bull. Amer. Meteor. Soc.*, **78**, 1069–1079. https://doi.org/10.1175/JCLI3321.1

Marsh, D. R., M. J. Mills, D. E. Kinnison, J.-F. Lamarque, N. Calvo, and L. M. Polvani, 2013: Climate change from 1850 to 2005 simulated in CESM1(WACCM). *J. Climate*, **26**, 7372–7391, https://doi.org/10.1175/JCLI-D-12-00558.1.

Marshall, G. J., A. Orr, N. P. M. van Lipzig, and J. C. King, 2006: The impact of a changing Southern Hemisphere annular mode on Antarctic Peninsula summer temperatures. *J. Climate*, **19**, 5388–5404, https://doi.org/10.1175/JCLI3844.1.

Ma, X., F. Xie, J. Li, X. Zheng, W. Tian, R. Ding, C. Sun, and J. Zhang, 2019: Effects of Arctic stratospheric ozone changes on spring precipitation in the northwestern United States. *Atmos. Chem. Phys.*, **19**, 861–875. https://doi.org/10.5194/acp-19-861-2019.

Min, S. K., and S. W. Son, 2013: Multimodel attribution of the Southern Hemisphere Hadley cell widening: Major role of ozone depletion. *J. Geophys. Res.*, **118**, 3007–3015, https://doi.org/10.1002/jgrd.50232.

Pawson, S., and B. Naukokat, 1999: The cold winters of the middle 1990s in the Northern Lower Stratosphere. *J. Geophys. Res.*, **104**, 14 209–14 222, https://doi.org/10.1029/1999JD900211.

Accepted for publication in *Journal of Climate*. DOI10.1175/JCLI-D-19-0292.1.

Polvani, L. M., D. W. Waugh, G. J. P. Correa, and S. W. Son, 2011: Stratospheric ozone depletion: The main driver of twentieth-century atmospheric circulation changes in the Southern Hemisphere. *J. Climate*, **24**, 795–812, https://doi.org/10.1175/2010JCLI3772.1.

Pu, X., Q. Chen, Q. Zhong, R. Ding, and T. Liu, 2019: Influence of the North Pacific Victoria mode on western North Pacific tropical cyclone genesis. *Climate Dyn.*, **52**(1-2): 245-256. DOI 10.1007/s00382-018-4129-z.

Ramaswamy, V., M. D. Schwarzkopf, and W. J. Randel, 1996: Fingerprint of ozone depletion in the spatial and temporal pattern of recent lower stratospheric cooling. *Nature*, **382**, 616–618, https://doi.org/10.1038/382616a0.

Randel, W. J., and F. Wu, 1999: Cooling of the Arctic and Antarctic polar stratospheres due to ozone depletion. *J. Climate*, **12**, 1467–1479. https://doi.org/10.1175/1520-0442(1999)012,1467:COTAAA.2.0.CO;2.

——, and ——, 2007: A stratospheric ozone profile data set for 1979–2005: Variability, trends, and comparisons with column ozone data. *J. Geophys. Res.*, **112**, D06313, https://doi.org/0.1029/ 2006JD007339.

Ravishankara, A. R., and Coauthors, 1994: Do hydrofluorocarbons destroy stratospheric ozone? *Science*, **263**, 71–5, https://doi.org/10.1126/science.263.5143.71.

——, J. S. Daniel, and R. W. Portmann, 2009: Nitrous oxide (N2O): the dominant ozone-depleting substance emitted in the 21st century. *Science*, **326**,

Accepted for publication in *Journal of Climate*. DOI10.1175/JCLI-D-19-0292.1.

123–125, https://doi.org/10.1126/science.1176985.

Reichler, T., J. Kim, E. Manzini, and J. Kröger, 2012: A stratospheric connection to Atlantic climate variability. *Nat. Geosci.*, **5**, 783–787, https://doi.org/10.1038/ngeo1586.

Russell, J. L., K. W. Dixon, A. Gnanadesikan, R. J. Stouffer, and J. R. Toggweiler, 2006: The Southern Hemisphere westerlies in a warming world: Propping open the door to the deep ocean. *J. Climate*, **19**, 6382–6390, https://doi.org/10.1175/JCLI3984.1.

Scaife, A. A., J. R. Knight, G. K. Vallis, and C. K. Folland, 2005: A stratospheric influence on the winter NAO and North Atlantic surface climate. *Geophys. Res. Lett.*, **32**, L18715, https://doi.org/10.1029/2005GL023226.

Schoeberl, M. R., and D. L. Hartmann, 1999: The dynamics of the stratospheric polar vortex and its relation to springtime ozone depletions. *Science*, 1991, **251**(4989): 46–52. DOI: 10.1126/science.251.4989.46.

Seviour, W. J. M., A. Gnanadesikan, and D. W. Waugh, 2016: The transient response of the Southern Ocean to stratospheric ozone depletion. *J. Climate*, **29**, 7383-7396, https://doi.org/10.1175/JCLI-D-16-0198.1.

Smith, K. L., and L. M. Polvani, 2014: The surface impacts of Arctic stratospheric ozone anomalies. *Environ. Res. Lett.*, **9**, 074015, doi:10.1088/1748-9326/9/7/074015.

Sheng, Z., Y. Jiang, L. Wan, and Z. Fan, 2015: A Study of Atmospheric Tem

Accepted for publication in *Journal of Climate*. DOI10.1175/JCLI-D-19-0292.1.

perature and Wind Profiles Obtained from Rocketsondes in the Chinese Midlatitude Region. *J. Atmos. Oceanic Technol.*, **32**, 722–735, https://doi.org/10.1175/JTECH-D-14-00163.1.

Solomon, S., 1990: Antarctic ozone: Progress towards a quantitative understanding. *Nature*, **347**, 354, https://doi.org/10.1038/347347a0.

——, 1999: Stratospheric ozone depletion: A review of concepts and history. *Reviews of Geophysics*, **37**, 275–316, https://doi.org/10.1029/1999RG900008.

——, J. Haskins, D. J. Ivy, and F. Min, 2014: Fundamental differences between Arctic and Antarctic ozone depletion. *Proc. Natl Acad. Sci.*, **111**, 6220–25, DOI: 10.1073/pnas.1319307111.

Son, S. W., and Coauthors, 2008: The impact of stratospheric ozone recovery on the Southern Hemisphere Westerly Jet. *Science*, **320**, 1486–1489.https://doi.org/10.1126/science.1155939.

——, and Coauthors, 2010: Impact of stratospheric ozone on Southern Hemisphere circulation change: A multimodel assessment. *J. Geophys. Res.*, **115**, D00M07, https://doi.org/10.1029/2010JD014271.

——, N. F. Tandon, L. M. Polvani, and D. W. Waugh, 2009: Ozone hole and Southern Hemisphere climate change. *Geophys. Res. Lett.*, **36**, L15705, https://doi.org/10.1029/2009GL038671.

Song, Y., and W. A. Robinson, 2004: Dynamical mechanisms for stratospheric

Accepted for publication in *Journal of Climate*. DOI10.1175/JCLI-D-19-0292.1.

influences on the troposphere. *J. Atmos. Sci.*, **61**, 1711–1725. https://doi.org/10.1175/1520-0469(2004)061,1711:DMFSIO.2.0.CO;2.

Song, L., Y. Li, W. Duan, 2016: The influence of boreal winter extratropical North Pacific Oscillation on Australian spring rainfall. *Climate Dyn.*, **47**, 1181–1196, https://doi.org/10.1007/s00382-015-2895-4.

Stolarski, R. S., and S. M. Frith, 2006: Search for evidence of trend slow-down in the long-term TOMS/SBUV total ozone data record: the importance of instrument drift uncertainty. *Atmos. Chem. Phys.*, **6**, 4057–4065, https://doi.org/10.5194/acp-6-4057-2006.

Thompson, D. W. J., S. Solomon, P. J. Kushner, M. H. England, K. M. Grise, and D. J. Karoly, 2011: Signatures of the Antarctic ozone hole in Southern Hemisphere surface climate change. *Nat. Geosci.*, **4**, 741–749, https://doi.org/10.1038/ngeo1296.

Tian, W., M. P. Chipperfield, D. S. Stevenson, R. Damoah, S. Dhomse, A. Dudhia, H. Pumphrey, and P. Bernath, 2010: Effects of stratosphere-troposphere chemistry coupling on tropospheric ozone. *J. Geophys. Res. Atmos.*, **115**, D00m04, https://doi.org/10.1029/2009jd013515.

Turner, J., and Coauthors, 2005: Antarctic climate change during the last 50 years. *Int. J. Climatol.*, **25**, 279–294. https://doi.org/10.1002/joc.1130.

van der A, R. J., M. A. F. Allaart, and H. J. Eskes, 2010: Multi sensor reanalysis of total ozone. *Atmos. Chem. Phys.*, **10**, 11277–11294. https://doi.or

Accepted for publication in *Journal of Climate*. DOI10.1175/JCLI-D-19-0292.1.

g/10.5194/acp-10-11277-2010.

——, ——, and ——, 2015: Extended and refined multi sensor reanalysis of total ozone for the period 1970–2012. *Atmos. Meas. Tech.*, **8**, 3021–3035., https://doi.org/10.5194/amt-8-3021-2015.

Vimont, D. J., D. S. Battisti, and A. C. Hirst, 2003: The seasonal footprinting mechanism in the CSIRO general circulation models. *J. Climate*, **16**, 2653–2667. https://doi.org/10.1175/1520-0442(2003)016<2653:TSFMIT>2.0.CO;2.

Wang, B., R. Wu, X. Fu, 2000: Pacific–East Asian teleconnection: how does ENSO affect East Asian climate? *J. Climate*, **13**(9): 1517–1536. https://doi.org/10.1175/1520-0442(2000)013<1517:PEATHD>2.0.CO;2

Waugh, D. W., L. Oman, P. A. Newman, R. S. Stolarski, S. Pawson, J. E. Nielsen, and J. Perlwitz, 2009: Effect of zonal asymmetries in stratospheric ozone on simulated Southern Hemisphere climate trends. *Geophys. Res. Lett.*, **36**, L18701, https://doi.org/10.1029/2009GL040419.

——, C. I. Garfinkel, and L. M. Polvani, 2015: Drivers of recent tropical expansion in the Southern Hemisphere: Changing SSTs or ozone depletion? *J. Climate*, **28**, 6581–6586, https://doi.org/10.1175/JCLI-D-15-0138.1.

——, A. H. Sobel, and L. M. Polvani, 2017: What is the polar vortex and how does it influence weather? *Bull. Amer. Meteor. Soc.*, **98**, 37–44. https://doi.org/10.1175/BAMS-D-15-00212.1.

Accepted for publication in *Journal of Climate*. DOI10.1175/JCLI-D-19-0292.1.

Woo, S. H., M. K. Sung, S. W. Son, and J. S. Kug, 2015: Connection between weak stratospheric vortex events and the Pacific decadal oscillation. *Climate Dyn.*, **45**, 3481–3492, https://doi.org/10.1007/ s00382-015-2551-z.

World Meteorological Organization (WMO), 2011: Scientific assessment of ozone depletion: 2010 Technical Report, Global Ozone Research and Monitoring Project Report No. 52 Geneva,Switzerland p 516.

Xia, Y., Y. Hu, Y. Huang, 2016: Strong modification of stratospheric ozone forcing by cloud and sea-ice adjustments. *Atmos. Chem. Phys.*, **16**, 7559–7567, https://doi.org/10.5194/acp-16-7559-2016.

Xie, F., and Coauthors, 2016: A connection from Arctic stratospheric ozone to El Niño‑Southern Oscillation. *Environ. Res. Lett.*, **11**, 124026, https://doi.org/10.1088/1748-9326/11/12/124026.

——, and Coauthors, 2017a: Variations in North Pacific sea surface temperature caused by Arctic stratospheric ozone anomalies. *Environ. Res. Lett.*, **12**, 114023, https://doi.org/10.1088/1748-9326/aa9005.

——, and Coauthors, 2017b: Delayed effect of Arctic stratospheric ozone on tropical rainfall. *Atmos. Sci. Lett.*, **18**, 409–416, https://doi.org/10.1002/asl.783.

——, and Coauthors, 2018: An advanced impact of Arctic stratospheric ozone changes on spring precipitation in China. *Climate Dyn.*, **1**, 4029–4041. https://doi.org/10.1007/s00382-018-4402-1.

Accepted for publication in *Journal of Climate*. DOI10.1175/JCLI-D-19-0292.1.

Xie, S.-P.,and S. G. H. Philander, 1994: A coupled ocean-atmosphere model of relevance to the ITCZ in the eastern Pacific. *Tellus*, **46A**, 340–350, https://doi.org/10.1034/j.1600-0870.1994.t01-1-00001.x.

Zhang, J., W. Tian, Z. Wang, F. Xie, and F. Wang, 2015: The influence of ENSO on northern midlatitude ozone during the winter to spring transition. *J. Climate*, **28**, 4774–4793, https://doi.org/10.1175/JCLI-D-14-00615.1.

——, ——, M. P. Chipperfield, F. Xie, and J. Huang, 2016: Persistent shift of the Arctic polar vortex towards the Eurasian continent in recent decades. *Nat. Climate Change*, **6**, 1094–1099, https://doi.org/10.1038/nclimate3136.

——, and Coauthors, 2018: Stratospheric ozone loss over the Eurasian continent induced by the polar vortex shift. *Nat. Commun.*, **9**, 206, https://doi.org/10.1038/s41467-017-02565-2.

Zhang, Y., J. M. Wallace, and D. S. Battisti, 1997: ENSO-like interdecadal variability: 1900–93. *J. Climate*, **10**, 1004–1020, https://doi.org/10.1175/1520-0442(1997)010<1004:ELIV>2.0.CO;2.

Figure captions

FIG. 1. Time series of Arctic (60°–90°N) TCO in March from the TOMS/SBUV (red line) and MSR (blue line) dataset.

FIG. 2. Correlation coefficients between Arctic –TCO (TOMS/SBUV dataset) in

Accepted for publication in *Journal of Climate*. DOI10.1175/JCLI-D-19-0292.1.

March and sea surface temperature (HadSST) in (a) March, (b) April, (c) May, (d) June, (e) July, and (f) August. (g–l) Same as (a–f), but the TCO data are from the MSR dataset and SST data are from the ERSSTv4 dataset. Dotted regions are statistically significant at the 95% confidence level according to Student's *t* test. The linear trends in all datasets have been removed.

FIG. 3. Correlation coefficients between Arctic –TCO in March and (a) geopotential height (color) and wind (vectors) at 300 hPa in June. (b) Same as (a) but for those at 850 hPa. In (a–b), the TCO data are from TOMS/SBUV dataset and geopotential height and wind data are from ERA-Interim dataset. (c–d) Same as (a–b), but the TCO data are from MSR dataset and geopotential height and wind data are from NCEP2 dataset. Dotted regions are statistically significant at the 95% confidence level.

FIG. 4. Blue lines are detrended and standardized time series of (a, d, g) 300 hPa geopotential height (H300, averaged over 30°–45°N, 130°E–180°), (b, e, h) 850 hPa geopotential height (H850, averaged over 30°–45°N, 130°E–180°), and (c, f, i) sea surface temperature (SST, averaged over 30°–40°N, 140°E–180°) in (a–c) April, (d–f) May and (g–i) June. Red lines in (a–i) are the time series of Arctic TCO in March from TOMS/SBUV dataset. The correlation coefficient (*r*) between red line and blue line in each panel is given in the title. *p* is the confidence level and *r* is statistically significant at the 99% confidence level when *p* is less than 0.01.

FIG. 5. Latitude-height cross-section of correlation coefficients between Arctic –TCO in March and zonal mean (a) temperature, (b) geopotential height, and (c) zonal wind

Accepted for publication in *Journal of Climate*. DOI10.1175/JCLI-D-19-0292.1.

in March. (d) and (e) are correlation coefficients between Arctic –TCO in March and zonal wind at 850 hPa in March and April, respectively. Dotted regions are statistically significant at the 95% confidence level.

FIG. 6. Correlation coefficients between Arctic –TCO in March and (a–c) SST (color) and winds (vectors) at 850 hPa in (a) April, (b) May, (c) June, and (d–f) geopotential height at 850 hPa in (d) April, (e) May, (f) June. Dotted regions are statistically significant at the 95% confidence level.

FIG. 7. Ray paths (coarse black lines) of Rossby waves (wavenumber 1) at 850 hPa. The wave source is over the eastern North Pacific (40°N, 140°W). (a), (b), (c), (d), (e), and (f) are for the 1st, 6th, 12th, 18th, 24th, and 30th days, respectively. Color regions indicate the distribution of the climatological (1979–2009) mean geopotential height (gpm) at 850 hPa in May-June. The red and white regions represent high and low geopotential height, respectively.

FIG. 8. Correlation coefficients between –H (geopotential height averaged over 30°–35°N, 145°–135°W) at 850 hPa in May and geopotential height at 850 hPa in (a) May and (b) June. Dotted regions are statistically significant at the 95% confidence level.

FIG. 9. Prescribed ozone forcing used in the numerical simulations. Blue solid line, red solid line, blue dashed line and red dashed line are March Arctic (60°–90°N) TCO prescribed in experiments R1, R2, R3 and R4, respectively. Black line is for CMIP5 ensemble mean ozone output.

Accepted for publication in *Journal of Climate*. DOI 10.1175/JCLI-D-19-0292.1.

FIG. 10. (a–c) SST (color) and horizontal wind (850 hPa, vector) differences between experiments R1 (ozone decreased by 15%) and R2 (ozone increased by 15%) in (a) April, (b) May, (c) June. (d–f) Geopotential height (850 hPa) difference between experiments R1 and R2 in (d) April, (e) May, (f) June. Dotted regions are statistically significant at the 90% confidence level.

FIG. 11. Same as FIG. 10, but for differences between experiments R3 (ozone decreased by 25%) and R4 (ozone increased by 25%).

FIG. 12. The spatial patterns of the (a) EOF1 mode and (b) EOF2 mode of SSTA field (after removing the globally averaged SSTAs) over North Pacific (124.5°E–100.5°W, 20.5°–65.5°N) in March. Variances explained by the EOF1 and EOF2 modes are 33.3% and 16.7%, respectively. (c–d) Detrended and standardized time series of (c) Arctic TCO and PC1, (d) Arctic TCO and PC2 in March. The signs of PC1 and PC2 are reversed to facilitate direct comparison. The correlation coefficients between TCO and PC1 and PC2 are –0.36 ($p<0.05$) and –0.39 ($p<0.05$), respectively.

FIG. 13. Correlation coefficients between Arctic –TCO (resi) in March and (a) geopotential height at 300 hPa, (b) geopotential height at 850 hPa, and (c) SST in June. Dotted regions are statistically significant at the 95% confidence level. (d, e, f) The explained variance (%) for (a, b, c), respectively.

Table 1. Fully coupled CESM-WACCM4 experiments with various prescribed ozone forcings.

Accepted for publication in *Journal of Climate*. DOI10.1175/JCLI-D-19-0292.1.

Experiment	Prescribed ozone forcing
R1	Decreased ozone run using case B_1955-2005_WACCM_SC_CN covering the period 1955–2005. Ozone forcing used is from CMIP5 ensemble mean ozone output (1955–2005) except that March ozone in the Arctic region 60°–90°N (from surface to the top of the atmosphere) is decreased by 15% compared with the CMIP5 ensemble mean ozone output (1955–2005), which was named ghg_forcing_1955-2005_CMIP5_EnsMean.c140414.nc, and can be downloaded at https://svn-ccsm-inputdata.cgd.ucar.edu/trunk/inputdata/atm/waccm/ub/ghg_forcing_1955-2005_CMIP5_EnsMean.c140414.nc. All natural and anthropogenic external forcing for R1 are based on original CESM input data.
R2	Same as R1, except that March ozone in the region 60°–90°N is increased by 15% compared with the CMIP5 ensemble mean ozone output.
R3	Same as R1, except that March ozone in the region 60°–90°N is decreased by 25% compared with the CMIP5 ensemble mean ozone output.
R4	Same as R1, except that March ozone in the region 60°–90°N is in

Accepted for publication in *Journal of Climate*. DOI10.1175/JCLI-D-19-0292.1.

creased by 25% compared with the CMIP5 ensemble mean ozone output.

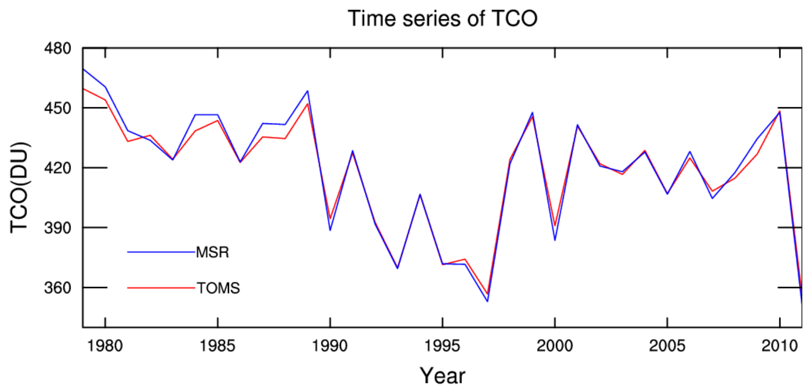

FIG. 1. Time series of Arctic (60°–90°N) TCO in March from the TOMS/SBUV (red line) and MSR (blue line) dataset.

Accepted for publication in *Journal of Climate*. DOI10.1175/JCLI-D-19-0292.1.

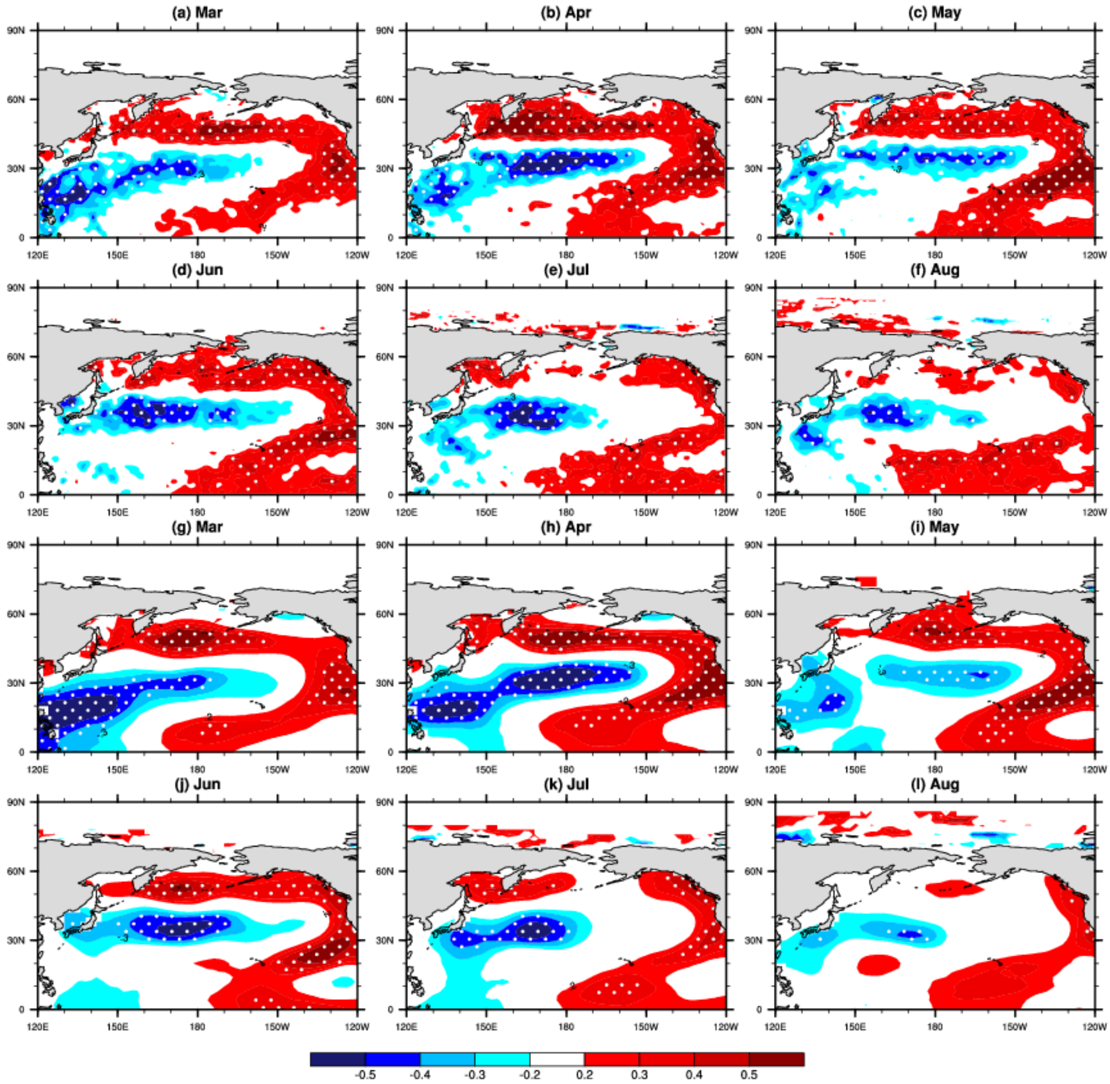

FIG. 2. Correlation coefficients between Arctic –TCO (TOMS/SBUV dataset) in March and sea surface temperature (HadSST) in (a) March, (b) April, (c) May, (d) June, (e) July, and (f) August. (g–l) Same as (a–f), but the TCO data are from the MSR dataset and SST data are from the ERSSTv4 dataset. Dotted regions are statistically significant at the 95% confidence level according to Student's *t* test. The linear trends in all datasets have been removed.

Accepted for publication in *Journal of Climate*. DOI10.1175/JCLI-D-19-0292.1.

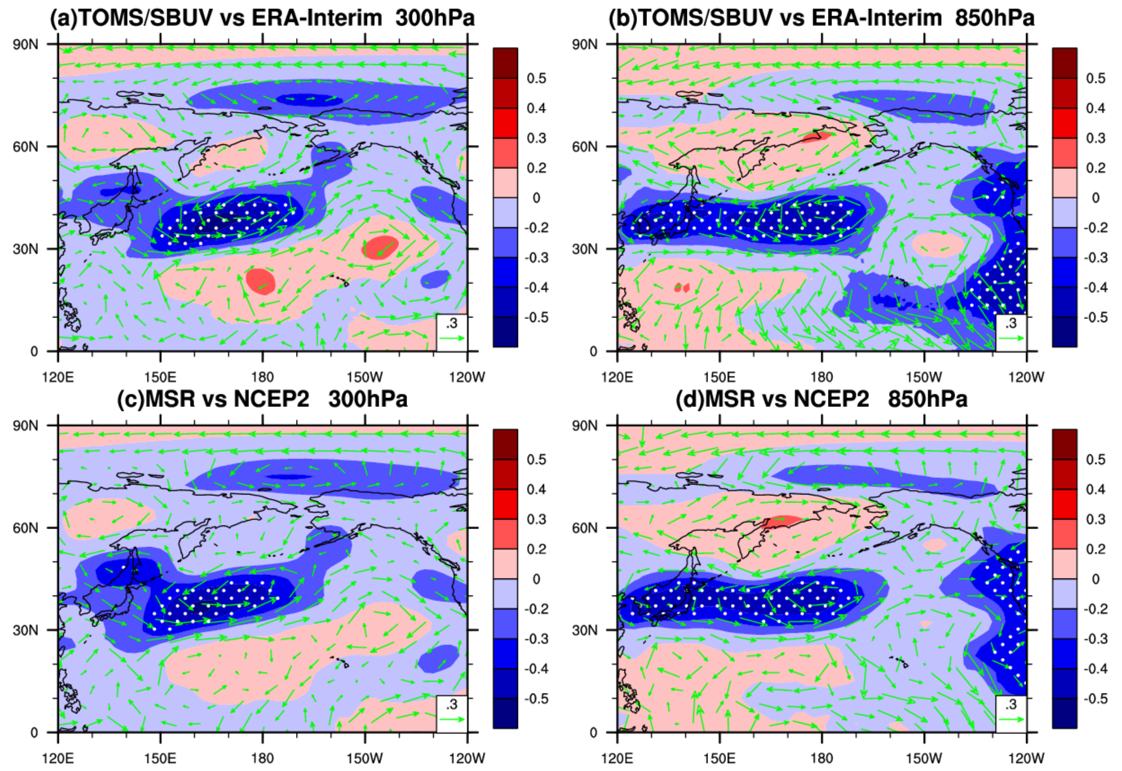

FIG. 3. Correlation coefficients between Arctic –TCO in March and (a) geopotential height (color) and wind (vectors) at 300 hPa in June. (b) Same as (a) but for those at 850 hPa. In (a–b), the TCO data are from TOMS/SBUV dataset and geopotential height and wind data are from ERA-Interim dataset. (c–d) Same as (a–b), but the TCO data are from MSR dataset and geopotential height and wind data are from NCEP2 dataset. Dotted regions are statistically significant at the 95% confidence level.

Accepted for publication in *Journal of Climate*. DOI10.1175/JCLI-D-19-0292.1.

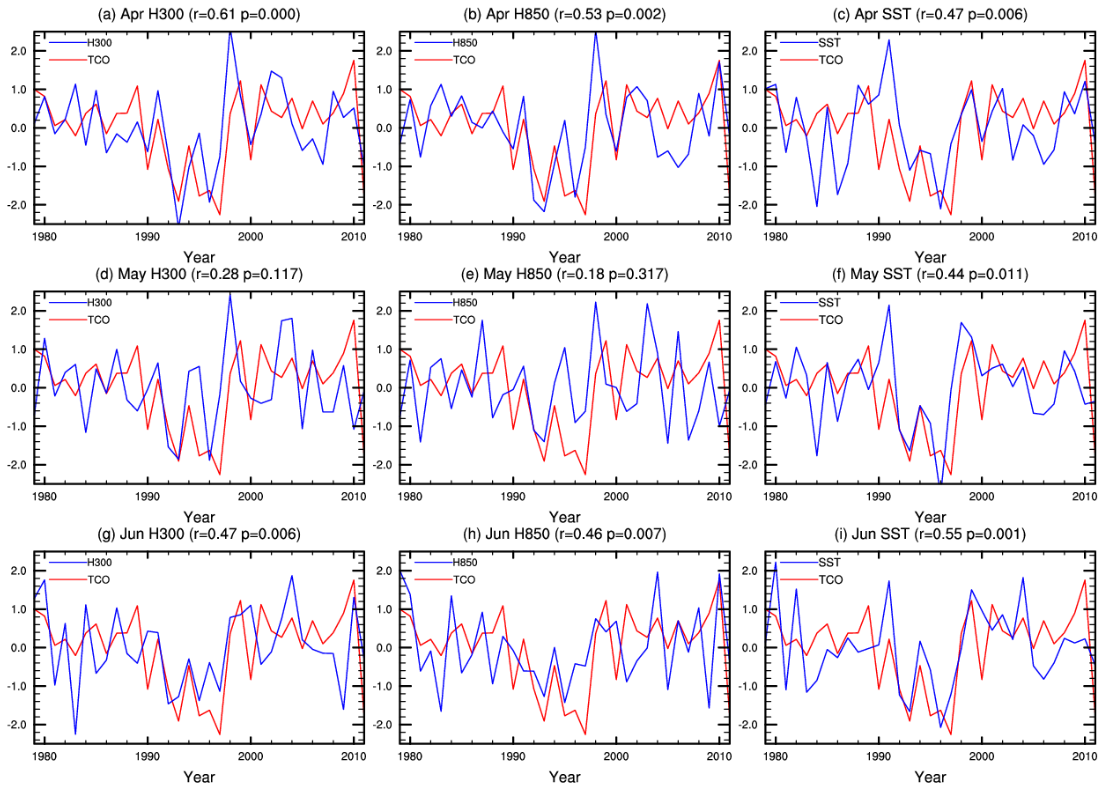

FIG. 4. Blue lines are detrended and standardized time series of (a, d, g) 300 hPa geopotential height (H300, averaged over 30°–45°N, 130°E–180°), (b, e, h) 850 hPa geopotential height (H850, averaged over 30°–45°N, 130°E–180°), and (c, f, i) sea surface temperature (SST, averaged over 30°–40°N, 140°E–180°) in (a–c) April, (d–f) May and (g–i) June. Red lines in (a–i) are the time series of Arctic TCO in March from TOMS/SBUV dataset. The correlation coefficient (*r*) between red line and blue line in each panel is given in the title. *p* is the confidence level and *r* is statistically significant at the 99% confidence level when *p* is less than 0.01.

Accepted for publication in *Journal of Climate*. DOI10.1175/JCLI-D-19-0292.1.

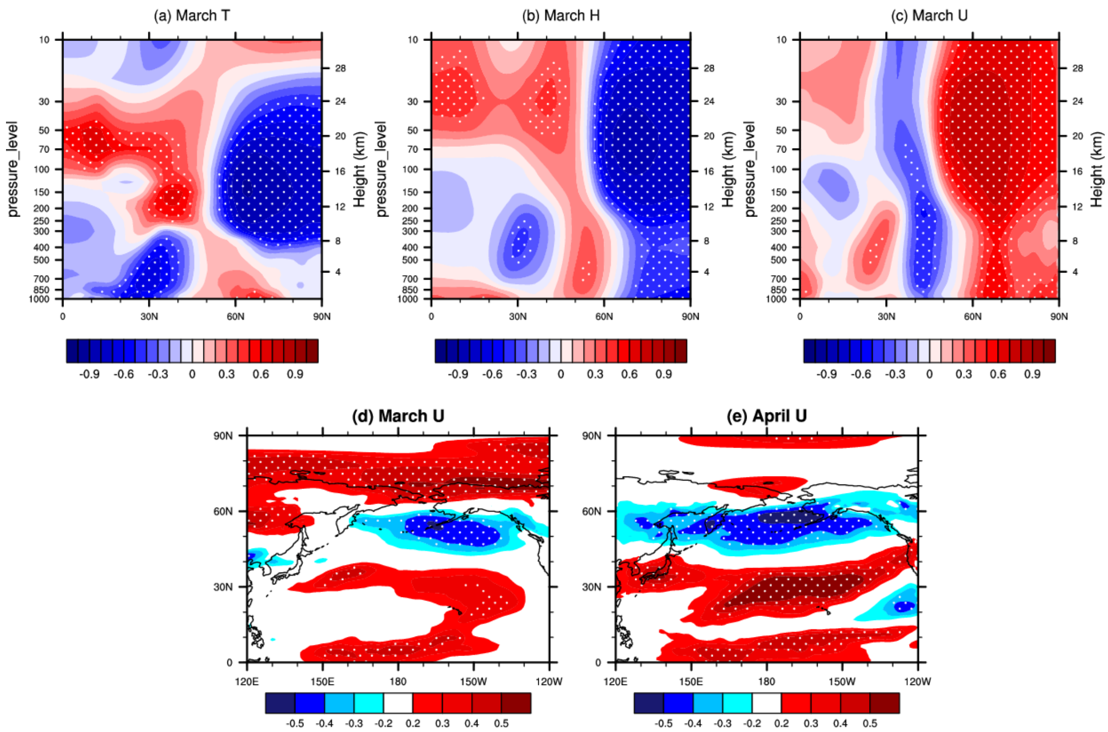

FIG. 5. Latitude-height cross-section of correlation coefficients between Arctic –TCO in March and zonal mean (a) temperature, (b) geopotential height, and (c) zonal wind in March. (d) and (e) are correlation coefficients between Arctic –TCO in March and zonal wind at 850 hPa in March and April, respectively. Dotted regions are statistically significant at the 95% confidence level.

Accepted for publication in *Journal of Climate*. DOI10.1175/JCLI-D-19-0292.1.

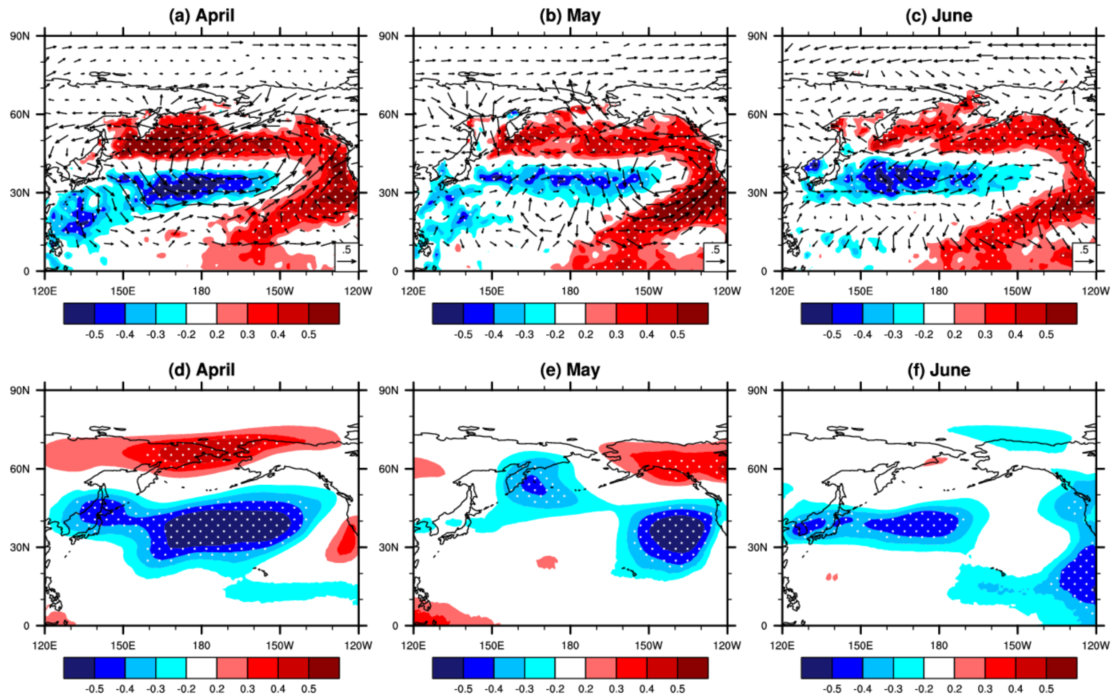

FIG. 6. Correlation coefficients between Arctic –TCO in March and (a–c) SST (color) and winds (vectors) at 850 hPa in (a) April, (b) May, (c) June, and (d–f) geopotential height at 850 hPa in (d) April, (e) May, (f) June. Dotted regions are statistically significant at the 95% confidence level.

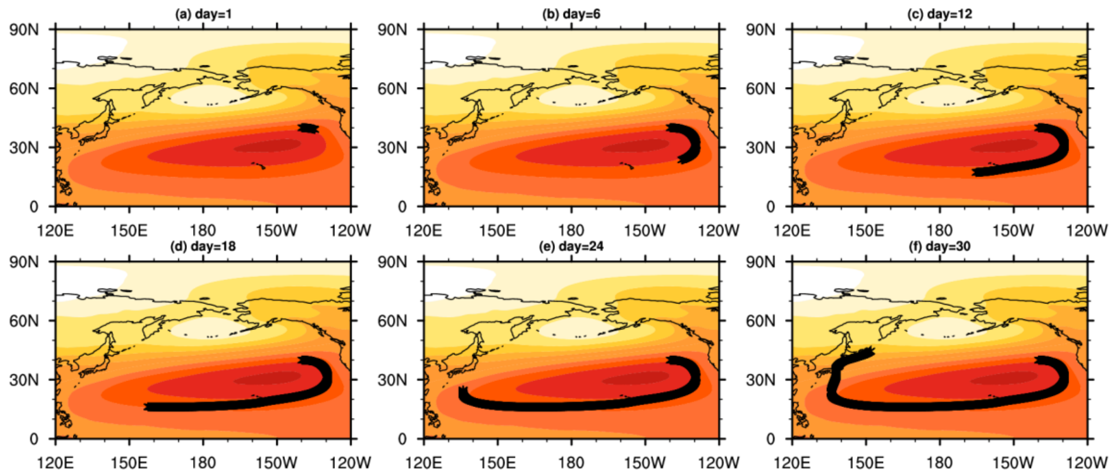

FIG. 7. Ray paths (coarse black lines) of Rossby waves (wavenumber 1) at 850 hPa. The wave source is over the eastern North Pacific (40°N, 140°W). (a), (b), (c), (d), (e), and (f) are for the 1st, 6th, 12th, 18th, 24th, and 30th days, respectively. Color regions

Accepted for publication in *Journal of Climate*. DOI10.1175/JCLI-D-19-0292.1.

indicate the distribution of the climatological (1979–2009) mean geopotential height (gpm) at 850 hPa in May-June. The red and white regions represent high and low geopotential height, respectively.

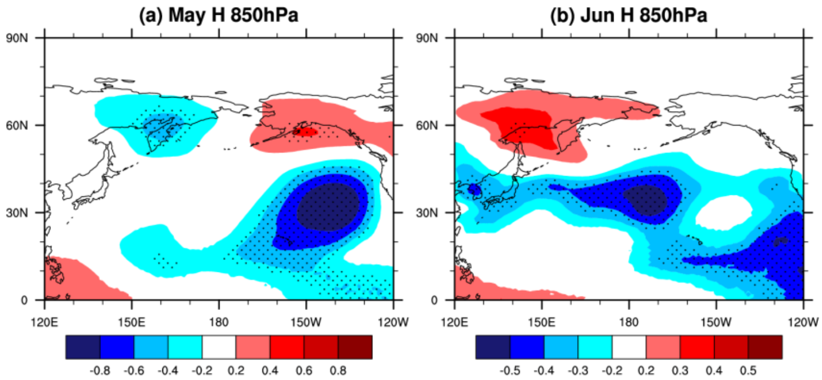

FIG. 8. Correlation coefficients between –H (geopotential height averaged over 30°–35°N, 145°–135°W) at 850 hPa in May and geopotential height at 850 hPa in (a) May and (b) June. Dotted regions are statistically significant at the 95% confidence level.

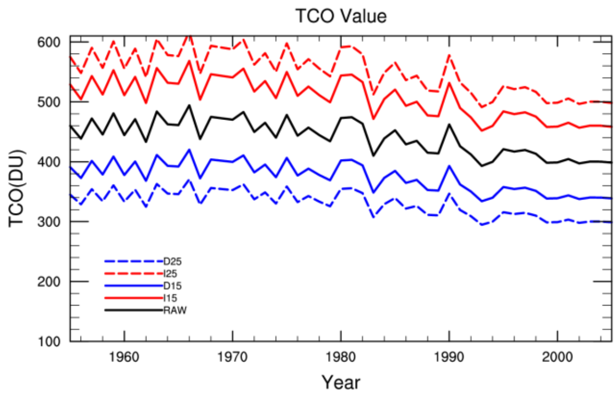

FIG. 9. Prescribed ozone forcing used in the numerical simulations. Blue solid line, red solid line, blue dashed line and red dashed line are March Arctic (60°–90°N) TCO prescribed in experiments R1, R2, R3 and R4, respectively. Black line is for CMIP5 ensemble mean ozone output.

Accepted for publication in *Journal of Climate*. DOI10.1175/JCLI-D-19-0292.1.

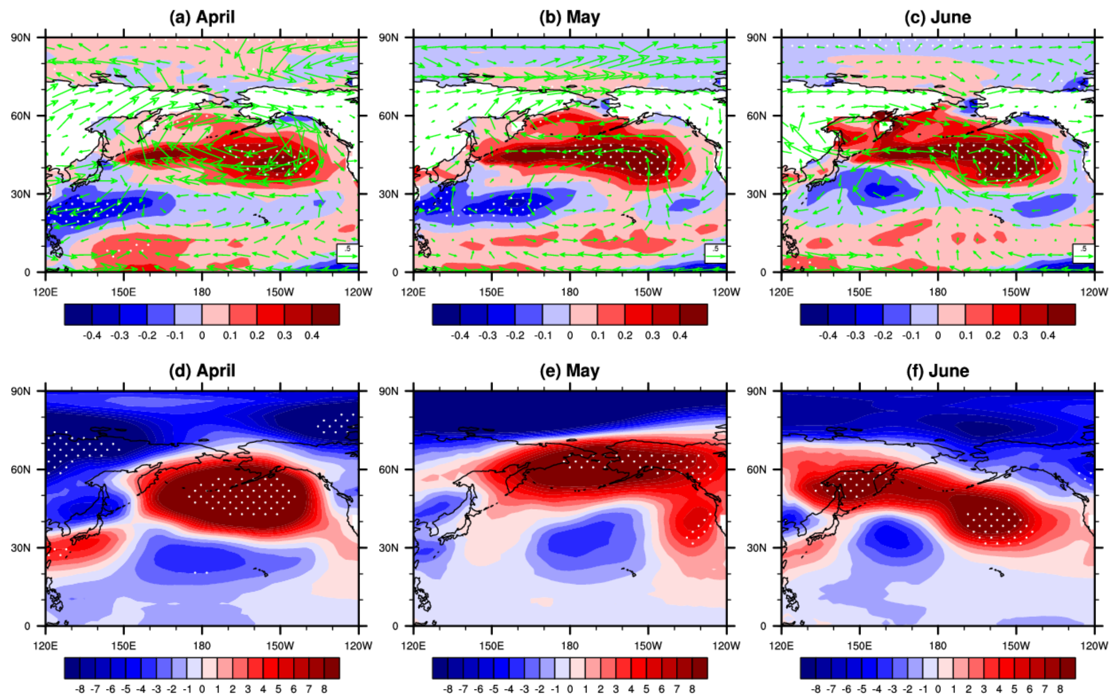

FIG. 10. (a–c) SST (color) and horizontal wind (850 hPa, vector) differences between experiments R1 (ozone decreased by 15%) and R2 (ozone increased by 15%) in (a) April, (b) May, (c) June. (d–f) Geopotential height (850 hPa) difference between experiments R1 and R2 in (d) April, (e) May, (f) June. Dotted regions are statistically significant at the 90% confidence level.

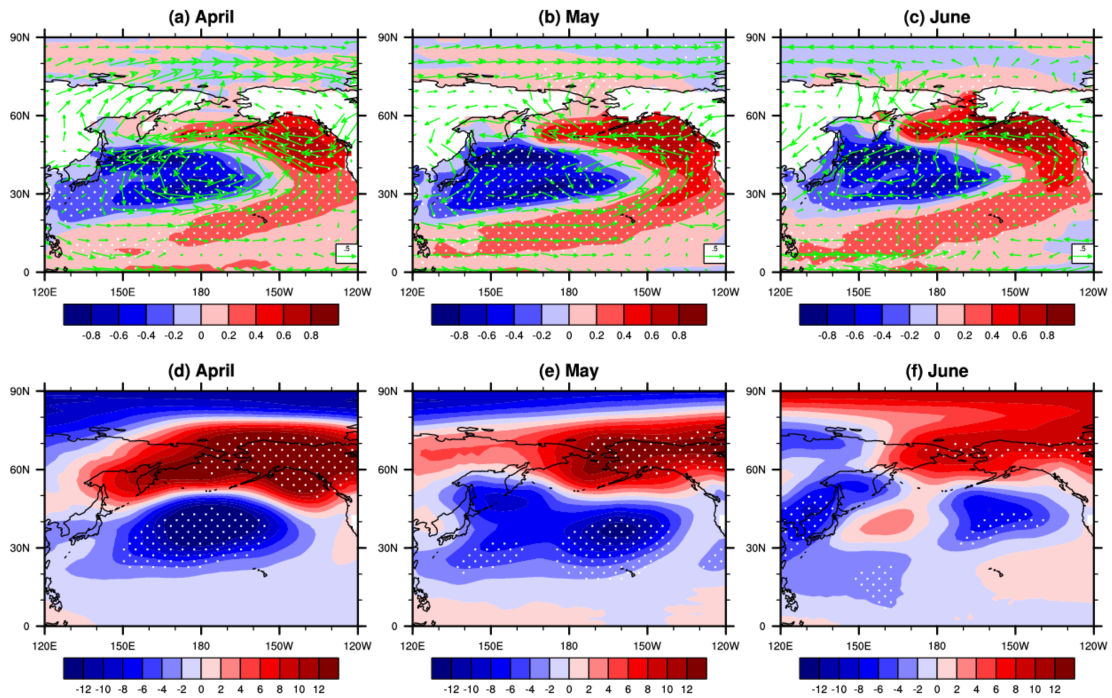

Accepted for publication in *Journal of Climate*. DOI10.1175/JCLI-D-19-0292.1.

FIG. 11. Same as FIG. 10, but for differences between experiments R3 (ozone decreased by 25%) and R4 (ozone increased by 25%).

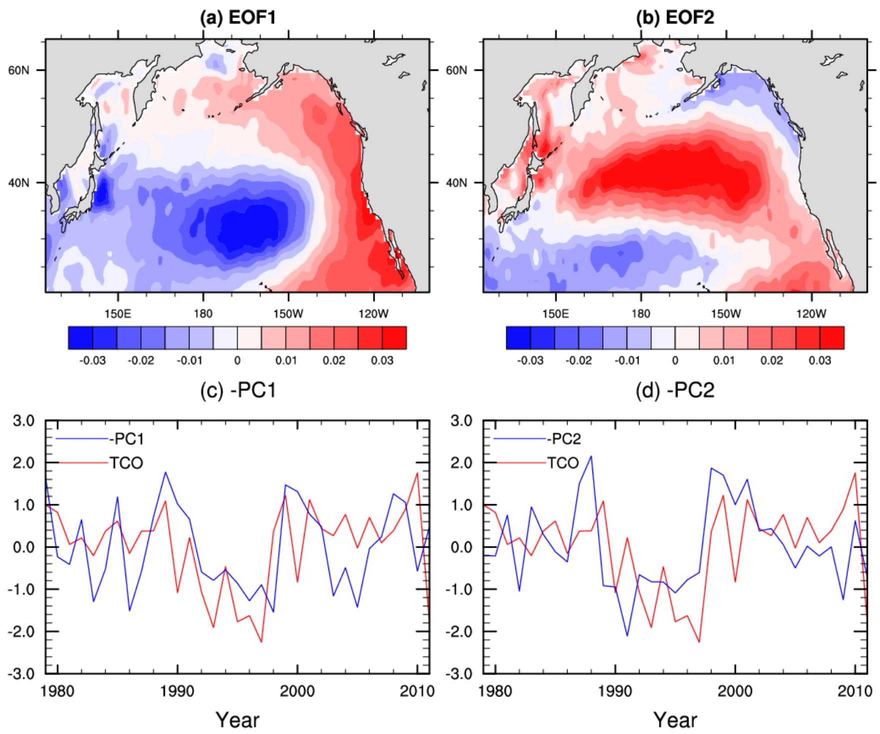

FIG. 12. The spatial patterns of the (a) EOF1 mode and (b) EOF2 mode of SSTA field (after removing the globally averaged SSTAs) over North Pacific (124.5°E–100.5°W, 20.5°–65.5°N) in March. Variances explained by the EOF1 and EOF2 modes are 33.3% and 16.7%, respectively. (c–d) Detrended and standardized time series of (c) Arctic TCO and PC1, (d) Arctic TCO and PC2 in March. The signs of PC1 and PC2 are reversed to facilitate direct comparison. The correlation coefficients between TCO and PC1 and PC2 are –0.36 ($p<0.05$) and –0.39 ($p<0.05$), respectively.

Accepted for publication in *Journal of Climate*. DOI 10.1175/JCLI-D-19-0292.1.

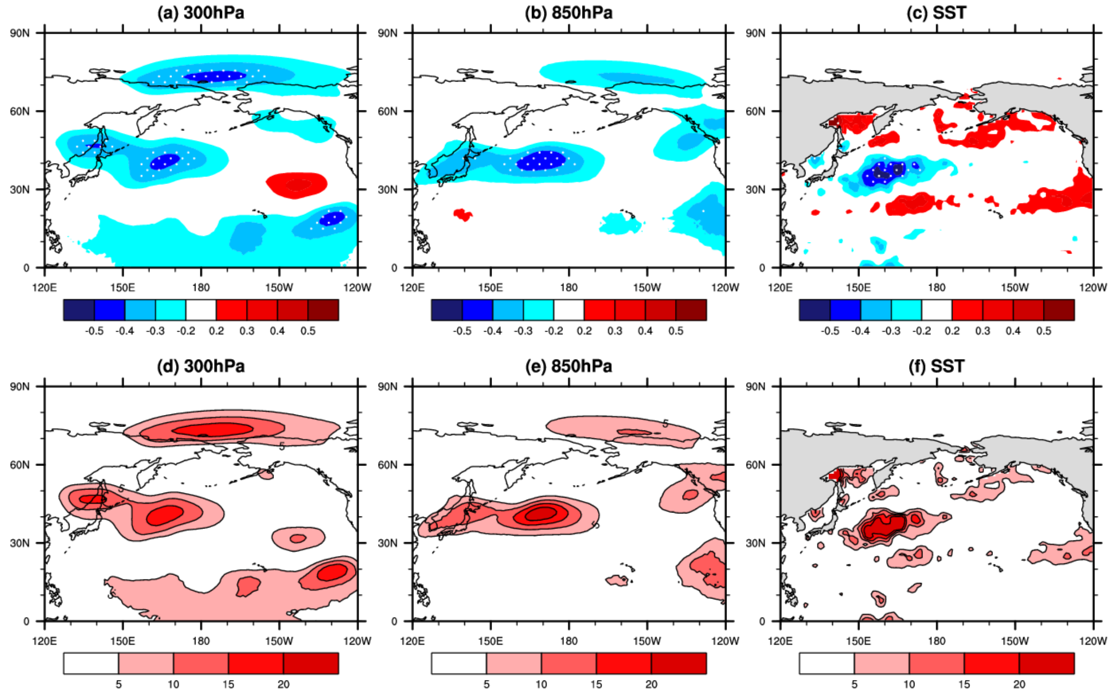

FIG. 13. Correlation coefficients between Arctic –TCO (resi) in March and (a) geopotential height at 300 hPa, (b) geopotential height at 850 hPa, and (c) SST in June. Dotted regions are statistically significant at the 95% confidence level. (d, e, f) The explained variance (%) for (a, b, c), respectively.

Accepted for publication in *Journal of Climate*. DOI10.1175/JCLI-D-19-0292.1.